Test particle simulation of non-ambipolar ion diffusion in tokamaks

T.P. Kiviniemi[a], J.A. Heikkinen[b], A.G. Peeters[c]

[a] Helsinki University of Technology, Association Euratom–TEKES, Department of Engineering Physics and Mathematics, Espoo, Finland
[b] VTT Chemical Technology, Association Euratom–TEKES, Espoo, Finland
[c] Max-Planck-Institut für Plasmaphysik, Garching, Germany

Abstract. The neoclassical return current and parallel viscosity due to the radial electric field (non-equilibrium poloidal rotation) in tokamaks are calculated using the 5-D (3-D in configuration space and 2-D in velocity space) Monte Carlo code ASCOT. Results are compared with the known neoclassical non-ambipolar return current expressions by Shaing [Phys. Fluids B **2** (1990) 2847] and Stringer [Nucl. Fusion **33** (1993) 1249] over a wide range of poloidal Mach numbers $M_p = E_r/(v_{ti}B_\theta)$ and for various collisionalities. Here, v_{ti} is the ion thermal velocity, E_r is the radial electric field and B_θ is the poloidal magnetic field. Quantitative differences exist due to a simpler collision operator and the various other approximations used in deriving the analytic expressions.

1. Introduction

Although the radial transport due to anomalous processes clearly exceeds the neoclassical transport in present tokamaks, the latter may play a dominant role in advanced confinement regimes, in radial current balance, bootstrap current and conductivity. In standard neoclassical theory, particle transport is automatically ambipolar and independent of radial electric field. However, this is not true in the presence of sources or sinks of toroidal momentum such as biased internal electrode or ion orbit loss current [1]. In experiments on TEXTOR [2], with an externally biased radial electric field, it has been shown that different theories for viscous damping of the poloidal rotation [3–7] are capable of predicting the radial conductivity better than to 'order of magnitude' level. The verification of these analytic expressions is important because one proposed explanation for the L–H transition is based on a multivalued balance between the non-ambipolar loss of fast ions and the return current [7] (Fig. 1). Such a balance with other types of non-ambipolar currents may play a role for internal thermal barriers in tokamaks. However, in the first self-consistent simulations of the ion orbit loss current and return current in a realistic geometry, bifurcation of solutions has not been observed [8, 9]. To investigate the bifurcation theory in more detail, it is essential to know the correct value of the neoclassical current, as well as the ion orbit loss current, as a function of various parameters such as electric field and collisionality. In this article, the return current is more accurately determined using the 5-D Monte Carlo code ASCOT [10]. The simulation is done using a full collision operator, without assuming the orbit widths to be small.

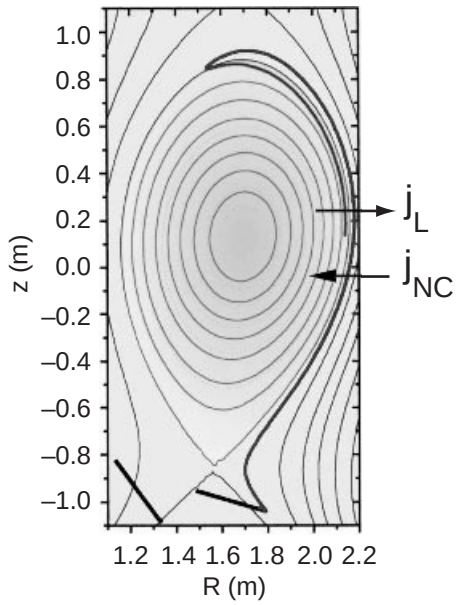

Figure 1. Current balance at the edge occurs when the ion orbit loss current j_L is balanced by the non-ambipolar neoclassical return current j_{NC}.

Both the parallel ion viscosity and the non-ambipolar ion neoclassical flux in the plateau and Pfirsch–Schlüter regimes with a given large poloidal rotation in the absence of orbit loss have been calculated analytically [11–13] from a Fokker–Planck equation with a simplified collision operator and in a simplified quasi-toroidal geometry. Here, somewhat arbitrarily, the parallel ion fluid velocity has been assumed to be zero. Steady state ion distributions in response to thermodynamical forces and to the electric field have been calculated from the kinetic equation for ions, but in the absence of any external force which would be required to sustain the given radial electric field, poloidal rotation and parallel flow velocity. This has been accomplished by expanding the guiding centre kinetic equation of ions to first order in the inverse aspect ratio with a fixed radial electric field, assuming a Maxwellian as the zeroth order ion distribution and neglecting the zeroth order parallel ion flow velocity. This assumption, which is validated by experimental observations, is made in many related analytic models. To find physical solutions, the ion fluxes obtained in this manner in Refs [4, 11, 13, 14] were then used to find a balance with external or internal forces ensuing from, for example, the externally applied radial electric field [2], torque from the orbit loss [7, 14] or inclusion of electron dynamics providing an ambipolar field [15]. In the derivation in Ref. [13], the poloidal variations of electrostatic potential, ion density and temperature were neglected, the distribution integrals were performed without non-resonant particles and in a restricted pitch angle space, and the finite orbit effects were omitted. Some of these effects are considered in later works of the author [16]. The solutions in Ref. [11] include the poloidal variations of the electrostatic field, density and temperature, and are based on full velocity integrals. As in Ref. [13], they include gradient and curvature drifts of the particles, but neglect finite orbit effects and radial variation of the electric potential along the particle orbits. In both Refs [11] and [13], the collision operator conserves momentum, but particle number and total energy were conserved in collisions only in Ref. [11]. Actually, the momentum is not exactly conserved because, in both cases, the parallel flow is assumed to be zero in the evaluation of the viscosity.

In this article, we calculate the parallel viscosity and the non-ambipolar ion radial current due to the radial electric field E_r by solving numerically the guiding centre equations of motion in toroidal co-ordinates for an ensemble of test ions with a fixed electrostatic potential $\Phi(r)$ which depends on radius r only. This method neglects the poloidal variation of the potential but includes that of density and temperature. We use the guiding centre Monte Carlo code ASCOT [10], where the finite orbit effects and full velocity and configuration space dynamics in a global tokamak geometry are taken into account. A momentum and energy conserving collision operator based on a binary collision model [17] is adopted to simulate ion–ion collisions. The collisions with electrons are omitted because the related friction leads to ambipolar fluxes which are not of interest to us at present. The comparison is best made in the absence of the orbit loss mechanism, and helps in assessing the validity of the various assumptions made in deriving the analytic expressions of the return current in Refs [11, 13].

Section 2 describes the Monte Carlo orbit following code, the tokamak model and the methods of calculating the ion orbit loss, radial non-ambipolar return flux and parallel viscosity. A comparison of the return ion flux with the analytic expressions is presented in Section 3.

2. Monte Carlo model of radial flux and parallel viscosity

2.1. Orbit integration

In this article, the orbit following Monte Carlo code ASCOT [10] is used to follow the guiding centre orbits of the test ions in the presence of collisions and an electric field. Inside the separatrix, the axisymmetric equilibrium field is given by

$$\boldsymbol{B} = g(\Psi_p)\boldsymbol{\nabla}\zeta + \mu_0 I(\Psi_p)\boldsymbol{\nabla}\theta + \delta(\Psi_p,\theta)\boldsymbol{\nabla}\Psi_p \qquad (1)$$

with Ψ_p the poloidal flux, θ the poloidal angle and ζ the toroidal angle. The co-ordinate system is a straight field line one, i.e. the safety factor $q(\Psi_p)$ gives the local helicity of a field line $q = d\zeta/d\theta$. The function $g(\Psi_p)$ is the poloidal current flowing outside the surface Ψ_p and $I(\Psi_p)$ is the toroidal current flowing inside the surface. The volume element is given by $d^3x = Jd\Psi_p d\theta d\zeta$, where the Jacobian is given by $J = (gq + I)/B^2$ [18]. The form of the latter defines the poloidal angle co-ordinate. The magnetic field strength $B(\Psi_p, \theta)$ is independent of ζ. The function $\delta(\Psi_p, \theta)$ describes the degree of non-orthogonality of the co-ordinate system.

In order to achieve the best accuracy and CPU time efficiency of the orbit solution, ASCOT applies

the magnetic field representation (1) with the Hamiltonian guiding centre equations [18] for the particle co-ordinates and parameters Ψ_p, θ, ζ, and $\rho_\parallel = m_i v_\parallel / e_i B$. Here, m_i, e_i and $v_\parallel$ are the ion mass, charge and parallel velocity component with respect to the magnetic field, respectively. The electrostatic potential in the equations is assumed to be of the form $\Phi(r, \theta)$. In this article, the poloidal dependence has been neglected. The simple fourth order Runge–Kutta method without error monitoring has, in addition to being very fast, proven satisfactory in reproducing the orbit topology consistently and conserving the constants of motion in tests where large numbers of consecutive collisionless guiding centre orbits were followed for test particles with varying initial parameters. As the numerical guiding centre solution method does not linearize the drift kinetic part of the equation, non-linear mechanisms and all zeroth and first order effects in ρ/L are kept. Here, L is a characteristic dimension over which the fields change and $\rho = m_i v_{ti}/e_i B$ is the Larmor radius.

2.2. Collision operator

During the guiding centre steps described above, the magnetic moment $\mu = m_i v_\perp^2/(2B)$, the toroidal canonical angular momentum $P_\phi = m_i R v_\parallel B_\phi / B + e_i \Psi_p$ and the total energy of the particle $\mathcal{E} = \mathcal{E}_k + e_i \Phi(r)$, where $\mathcal{E}_k = m_i v^2/2$, remain constant within the accuracy of the integration. Here, $v_\perp$ is the perpendicular component of the particle velocity with respect to the magnetic field, v is the velocity composed of the gyro-motion and parallel motion, and B_ϕ is the toroidal component of the magnetic field. However, because of collisions, μ, P_ϕ and $\mathcal{E}_k$ are changed after each time step. These changes lead to neoclassical diffusion of the particle in a torus. The collisional changes are calculated instantaneously by keeping the particle guiding centre position in the configuration space intact. Thus, the classical gyrotropic diffusion [19] of the particle is not included.

A binary collision model, exploited earlier in particle-in-cell and gyrokinetic simulations [17], is used to model ion–ion collisions. The simulation region is divided into poloidal and radial cells with size such that the plasma parameters do not vary significantly inside the cells. Particles in each cell are paired randomly and small angle collisions are performed pairwise. The chosen collision operator conserves the number of particles, the total momentum and the total energy quasi-locally. Using this method with fixed radial electric field and in the absence of other forces, test particle flux parallel to the magnetic field arises to compensate for the $\boldsymbol{E}\times\boldsymbol{B}/B^2$ and diamagnetic poloidal rotation resulting from the zero radial ion flux and thus satisfying the stationary conditions required by the fully momentum conserving collision operator in the absence of electron effects. In order to compare the results with analytic estimates for small parallel velocity, the measurement has to be done before significant parallel velocity has developed.

Alternatively, in the calculation of radial current, an ad hoc parallel force can be used to support stationary solutions with non-zero rotation. This can be done most efficiently by using a test particle collision operator instead of a full collision model. This operator keeps the test particles in a thermal bath of background ion species at temperature T_j. Here, momentum is not fully conserved but an external force $\boldsymbol{F}_{ii} = \int m_i \boldsymbol{v}_i [C(F_{Mi}, f_i) - C(f_i, f_i)]\, d\boldsymbol{v}$ appears in addition to that ensuing from the full momentum conserving collision operator $C(f_i, f_i)$. Here f_i is the total ion distribution function, F_{Mi} the Maxwellian part of the ion distribution and $C(F_{Mi}, f_i)$ the test particle collision operator. This force is proportional to the mean parallel ion flow $u_{\parallel i}$. This approximation is based on the assumption that the fluxes are mainly determined from the lowest order moments of the Boltzmann equation. This is verified by comparing the results of this method with simulations done using the momentum conserving binary collision model (parameters as in Section 3). In Fig. 2, it is shown that both methods give initially the same radial ion flux before the parallel velocity develops in the momentum conserving case and the flux decays.

The calculation of parallel viscosity can only be done with the binary collision model and, also, in the simulation of radial current it is used as the main method.

2.3. Calculation of the non-ambipolar radial flux

We calculate the non-ambipolar flux surface averaged ion radial current density due to a fixed radial electric field E_r with a Monte Carlo technique from the number of particles ΔN crossing a flux surface during time Δt as

$$j_{NC} = \frac{e_i}{A}\frac{\Delta N}{\Delta t} \tag{2}$$

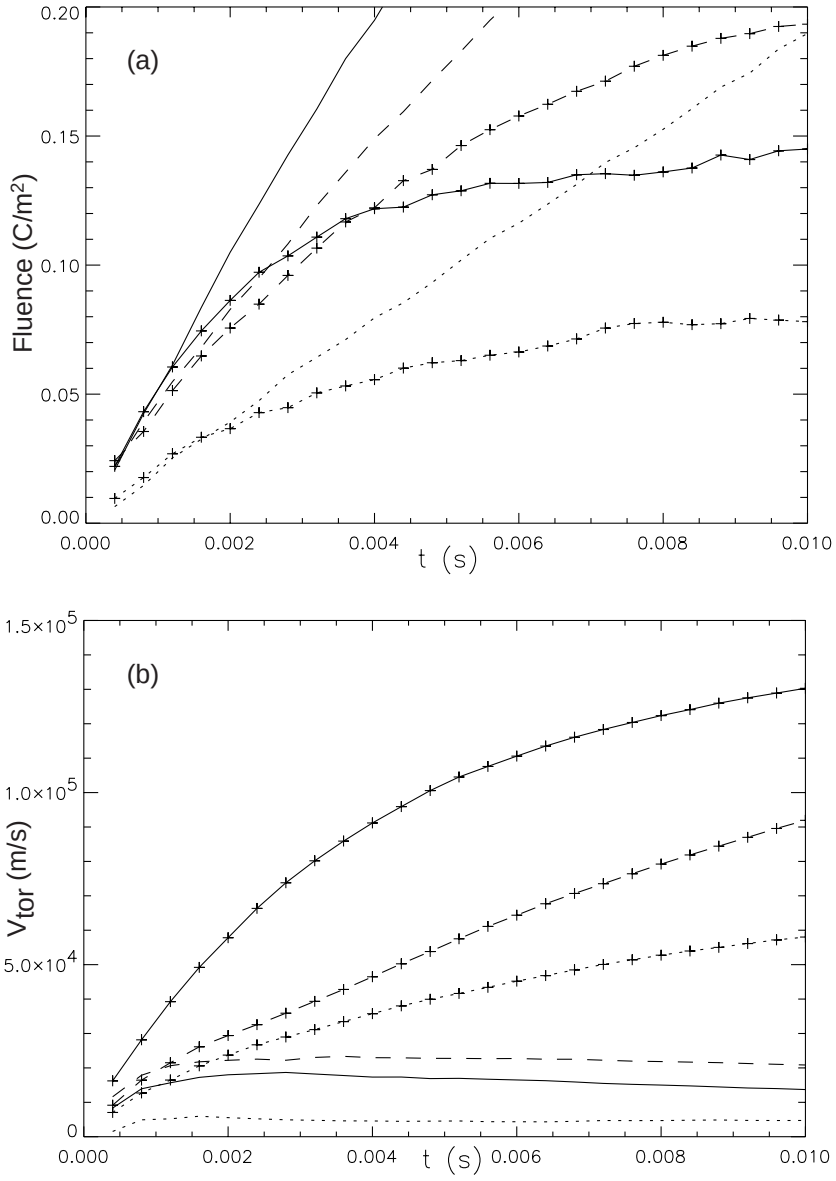

Figure 2. (a) Particle fluence and (b) toroidal velocity for $n = 5 \times 10^{19}$ m^{-3} and $T = 300$ eV with electric fields $E_r = 15$ kV/m (dotted curves), $E_r = 30$ kV/m (solid curves) and $E_r = 60$ kV/m (dashed curves). Curves with crosses are calculated with the momentum conserving binary collision operator and curves without crosses are calculated with the fixed background collision model.

where A is the area of the flux surface. The simulation is done for zero density and temperature gradients in order to neglect the influence of gradients. Test particles are initialized over a regime wide enough to avoid a decay of flux due to the exhaust of test particles. This would occur if the outermost particles have time enough to reach the flux surface where the flux is measured. A test particle in the simulation represents a group of initially uniformly (in configuration space) and Maxwellian (in velocity space) distributed particles, and it is weighted with a number that corresponds to the relative phase space volume of the initial position and velocity of the particle. To show the convergence of the method, the accumulated fluence of the particles per area element $e_i \Delta N/A$ is plotted as a function of time in Fig. 3.

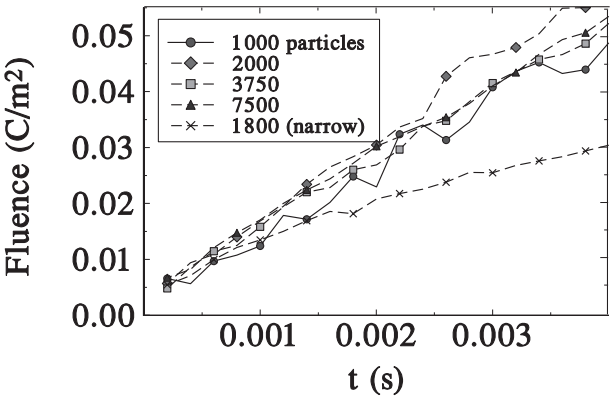

Figure 3. Particle fluence as a function of time for various sizes of test particle ensemble. Statistical noise decreases when the number of test particles is increased. If the initialization regime is too narrow, the fluence grows with a decaying rate.

Here, were have initialized 1800–7500 particles in a region $\rho_N = 0.3$–0.55 in normalized radius $\rho_N = r/a$. Particles are distributed uniformly in 10–20 poloidal angles between 0 and 2π, in 10–20 pitches between -1 and 1, and in 10–30 radius slots. The fluence is measured at the radius location $\rho_N = 0.5$ over 4 ms. The pedestal at the beginning is due to initialization. We see that already with 3750 particles we obtain a smoothly growing fluence. In addition, a case with 1800 particles is shown in Fig. 3, where a too narrow initialization regime ($\rho_N = 0.46$–0.52) has been applied. The fluence here grows with a decaying rate since the test particles from the edge of the simulation regime can reach the flux measurement radius within the simulation time. In this example a test particle collision model with fixed background was used. When a binary collision model is used, at least ten times more particles are needed for convergent results.

2.4. Calculation of the parallel viscosity

Starting from the momentum balance equation

$$n_i m_i \frac{d\boldsymbol{u}_i}{dt} = e_i n_i (\boldsymbol{E} + \boldsymbol{u}_i \times \boldsymbol{B}) - \boldsymbol{\nabla} p_i - \boldsymbol{\nabla} \cdot \boldsymbol{\Pi}_i + \boldsymbol{F}_i \tag{3}$$

one can calculate the parallel viscosity using the Monte Carlo technique. Here n_i and $\boldsymbol{u}_i$ are the ion fluid density, and velocity, respectively. $\boldsymbol{E} = -\boldsymbol{\nabla}\Phi$ is an electrostatic field, p_i is the scalar pressure and $\boldsymbol{\Pi}_i$ is the viscous stress tensor of fluid ions. $\boldsymbol{F}_i$ is the friction force arising from collisions of the ion with the other species. Assuming that the electric field is electrostatic and there are no other external forces, one can take an inner product with $\boldsymbol{B}$ in Eq. (3) and, after flux surface averaging, the equation for the parallel flow dynamics is

$$\begin{aligned}\left\langle m_i \frac{\partial (n_i \boldsymbol{B}\cdot\boldsymbol{u}_i)}{\partial t}\right\rangle = &-\langle \boldsymbol{B}\cdot\boldsymbol{\nabla}\cdot\boldsymbol{\Pi}_i\rangle \\ &-\langle m_i(\boldsymbol{B}\cdot\boldsymbol{u}_i)\boldsymbol{\nabla}\cdot(n_i\boldsymbol{u}_i)\rangle \\ &-\langle n_i m_i \boldsymbol{B}\cdot\boldsymbol{u}_i\cdot\boldsymbol{\nabla}\boldsymbol{u}_i\rangle \end{aligned} \tag{4}$$

where the right hand side can be interpreted as the total parallel viscosity value, consisting of the standard parallel viscosity and convection terms valid for arbitrarily large centre of mass velocities. The standard parallel viscosity in terms of pressure anisotropy is

$$\langle \boldsymbol{B}\cdot\boldsymbol{\nabla}\cdot\boldsymbol{\Pi}_i\rangle = \left\langle (p_\perp - p_\parallel)\frac{\boldsymbol{B}\cdot\boldsymbol{\nabla}B}{B}\right\rangle \tag{5}$$

and it can be calculated directly from the code in terms of the statistically measured pressure components $p_\parallel = \int m(v_\parallel - u_\parallel)^2 f\, d^3v$ and $p_\perp = \int [m(\boldsymbol{v}_\perp - \boldsymbol{u}_\perp)^2/2] f\, d^3v$, i.e. parallel and perpendicular pressure, respectively. In a quasi-toroidal system, Eq. (4) can be written as

$$\begin{aligned}\frac{\partial}{\partial t}\langle nBu_\parallel\rangle = &-\left\langle \frac{B}{rR}\frac{\partial}{\partial r}(rRnu_r u_\parallel)\right\rangle \\ &+\left\langle 2nu_\theta u_\parallel \frac{B\sin\theta}{R}\right\rangle \\ &-\left\langle (u_\theta^2 + u_\phi^2)\frac{B_\theta \sin\theta}{R}\right\rangle \\ &-\left\langle (p_\perp - p_\parallel)\frac{\boldsymbol{B}_\theta\cdot\boldsymbol{\nabla}B}{B}\right\rangle \\ &-\left\langle nu_r\left(\frac{B_\phi u_\phi}{R}\cos\theta + \frac{B_\theta u_\theta}{r}\right)\right\rangle \end{aligned} \tag{6}$$

where u_r, u_θ and u_ϕ are the radial, poloidal and toroidal components of flow velocity, respectively. All the velocity components, as well as $p_\parallel$ and $p_\perp$, are calculated from the code as time and ensemble averages of the particle velocities.

3. Simulation of the neoclassical return current and the parallel viscosity

In this section, the results from the analytic expressions in Eqs (9), (10) and (12) of the Appendix

for the return current and parallel viscosity are compared with the results from the ASCOT simulation. Circular symmetry with no Shafranov shift is assumed in the simulations, consistent with the assumptions in the derivation of the analytic forms. We determine the flux at the normalized radius $\rho_N = 0.5$ as an average over a time which is short enough (typically milliseconds) so that the boundaries of the initialization regime do not have an influence on the results. Temperature, density and current density profiles are assumed to be flat in order to ignore the influence of gradients. Parameters similar to those of ASDEX Upgrade, $a = 0.5$ m, $I_p = 1$ MA and $B_\phi = -2.5$ T, are used for minor radius, plasma current and toroidal magnetic field on the axis, respectively. The major radius, however, is chosen to have a larger value ($R = 3$ m) in order to neglect the effect of small aspect ratio corrections (the analytic results were derived in the large aspect ratio limit). The background ion density in the basic case is $n = 5 \times 10^{19}$ m^{-3} and the temperature $T = 150$ eV, corresponding to a normalized collisionality $\nu_{*i} = 22.6$. Collisionality is varied by changing both the temperature and the density.

Figures 4 and 5 show the return current from ASCOT and from the analytic expressions as a function of the poloidal Mach number $M_p = E_r/v_{ti}B_\theta$. In calculating the currents in Fig. 4, the collisionality is changed by varying the density with values $n = 2 \times 10^{19}$, $n = 5 \times 10^{19}$ and $n = 10 \times 10^{19}$ m^{-3} at a temperature $T = 150$ eV, corresponding to normalized collisionalities $\nu_{*i} = 9.4$, 23 and 45, respectively. In Figs 5(a) and (b), the density is $n = 5 \times 10^{19}$ m^{-3}, and the temperature has the values $T = 100$ eV and $T = 300$ eV with collisionalities $\nu_{*i} = 49$ and 6, respectively. We see that the best match between the currents from the ASCOT simulation and from the analytic expression (9) by Stringer is in Fig. 4(b), which is the case in the plateau regime not too near either the banana or Pfirsch–Schlüter regime. Comparison of Figs 5(a) and 4(c) suggests that the match between the curves depends on ν_{*i}, not the density or temperature alone. In addition Figs 5(b) and 4(a) have similar collisionalities and the relations between the curves are similar in both figures. Since the collisionality regime near the limit of banana regime is most interesting when the bifurcation theory of Ref. [7] is considered, we make the comparison of neoclassical return currents for a temperature $T = 300$ eV with a density $n = 2 \times 10^{19}$ m^{-3}, corresponding to a collisionality $\nu_{*i} = 2.5$. In Fig. 5(c), Shaing's result and the ASCOT simulation give nearly equally high maxima for the radial current although not for the same poloidal Mach number. Closer to the banana regime, the separation between the ASCOT result and Eq. (9) increases because toroidal trapping effects make the expansion in powers of inverse aspect ratio with a Maxwellian zeroth order distribution invalid in the derivations in Refs [11, 12]. Somewhat surprisingly, there is no such tendency of ASCOT results to deviate from

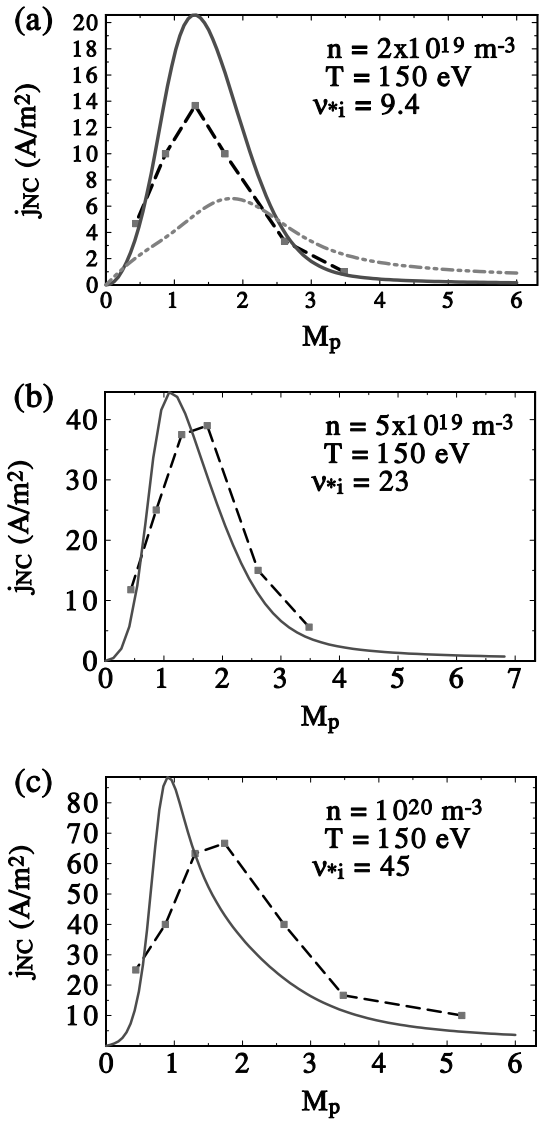

Figure 4. Neoclassical current j_{NC} as a function of poloidal Mach number for different densities (a) $n = 2 \times 10^{19}$ m^{-3}, (b) $n = 5 \times 10^{19}$ m^{-3} and (c) $n = 10 \times 10^{19}$ m^{-3}. Here, the dashed lines with squares are the ASCOT results, the chain curve (shown only for lowest ν_{*i}) is calculated from the expression of Shaing and the solid curves from the expression of Stringer.

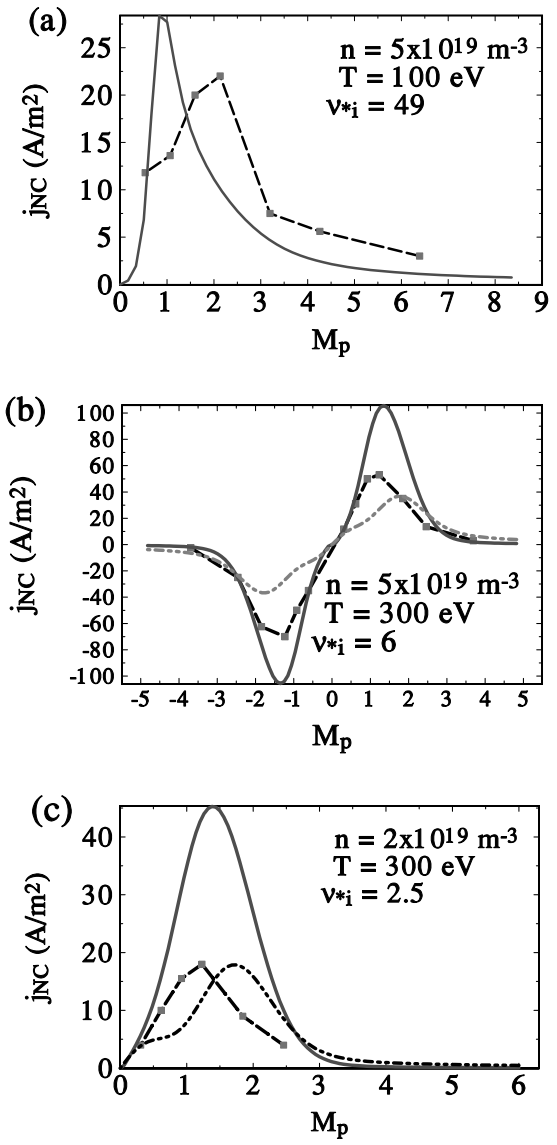

Figure 5. Neoclassical current j_{NC} as a function of poloidal Mach number for different temperatures (a) $T =$ 100 eV and (b) $T = 300$ eV with density $n = 5{\times}10^{19}$ m^{-3} and (c) for the low collisionality case with $T = 300$ eV and $n = 2 \times 10^{19}$ m^{-3}. The meaning of the lines is the same as in Fig. 4.

Eq. (12) by Shaing for this range of collisionality. This should be regarded as a pure artefact because the same expansion is used in both analytic models. The location of the maximum of the current in Eq. (12) by Shaing shifts strongly to higher values of M_p when collisionality is increased, but for the current in Eq. (9) by Stringer, the maximum is at $M_p \approx 1$ for all cases. The latter is in better agreement with the numerical results, which show only a small shift of the maximum.

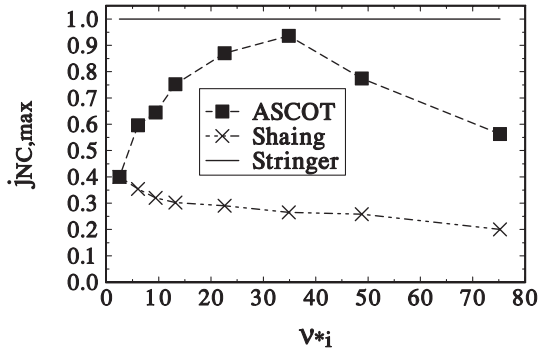

Figure 6. Comparison of the maximum values of the current j_{NC} from the different methods. Shaing's expression gives the lowest maximum, but near the banana regime agreement with the numerical result is better. The maxima are normalized to the maximum of $j_{NC,str}$.

In Fig. 6, the maxima of the three expressions for return current are compared. In all the cases shown, Eq. (12) by Shaing gives the lowest maximum, but it approaches the numerical result when collisionality decreases. Deviations in the collisional regime are natural since this expression of Shaing does not include Pfirsch–Schlüter effects and, thus, does not give the total radial current. In addition, some of the differences obtained here may be explained by the different collision models used. In the derivations of Eqs (9)–(12), essentially the Krook model (in a somewhat modified form) for collisions was applied. Although with proper coefficients the Krook model is known [20] to reproduce viscosity and fluxes obtained from a more complete collision operator in a relatively wide collision regime for weak rotation, in the present case of large poloidal Mach number its validity is not guaranteed. The main difference between the expressions of Shaing and Stringer is most probably that only the latter is based on full velocity integrals, which might be the reason why it has a tendency to agree better with the numerical results which also take into account the whole velocity space.

As an example of the importance of convection and compressibility in the calculation of total parallel viscosity we compare in Fig. 7 the numerical ASCOT simulation of total parallel viscosity, i.e. the RHS of Eq. (4), with the parallel viscosity calculated numerically from Eq. (5) and analytically from Eq. (10). Here, the density is $n = 5 \times 10^{19}$ m^{-3}, and temperatures (a) 100 eV and (b) 200 eV correspond to the collisionalities $\nu_{*i} = 46$ and 12, respectively, the first being in the Pfirsch–Schlüter regime and

the latter in the plateau regime. The measurement is made transiently after the effect of initialization has been lost, but before any significant parallel velocity develops. This causes an inaccuracy which can be 20–30%. Both in the Pfirsch–Schlüter regime and in the plateau regime, for large poloidal Mach numbers, the standard parallel viscosity $\langle \boldsymbol{B} \cdot \boldsymbol{\nabla} \cdot \boldsymbol{\Pi}_i \rangle$ has a different sign than the sum of all the RHS terms, i.e. its effect is to resist the growth of the parallel rotation which is driven by the other terms. The reason for this qualitative difference in results may be the strong poloidal dependence of density which develops for large M_p and is neglected in Ref. [23]. This is under investigation and will be published elsewhere. With small poloidal rotation, parallel viscosity also drives parallel rotation, which leads to the decay of poloidal rotation. Here, a good agreement between the numerically obtained standard parallel viscosity and the analytic result is found in the plateau regime. Although, in our simulations, we can clearly see the strong effect of both convection and compression in the parallel momentum balance for large values of M_p, for the poloidal component of the momentum equation in the case of zero radial current the effect of convection can be shown to be weak [21]. In Fig. 7(c), the same comparison is made for the low collisionality case, i.e. for a temperature $T = 300$ eV also with a density $n = 2 \times 10^{19}$ m^{-3} corresponding to a collisionality $\nu_{*i} = 2.5$. Again, we find that the parallel viscosity from the code changes sign for large poloidal Mach numbers but, somewhat surprisingly, a fairly good agreement can be found between Shaing's expression for the standard parallel viscosity and the ASCOT result for the total parallel viscosity.

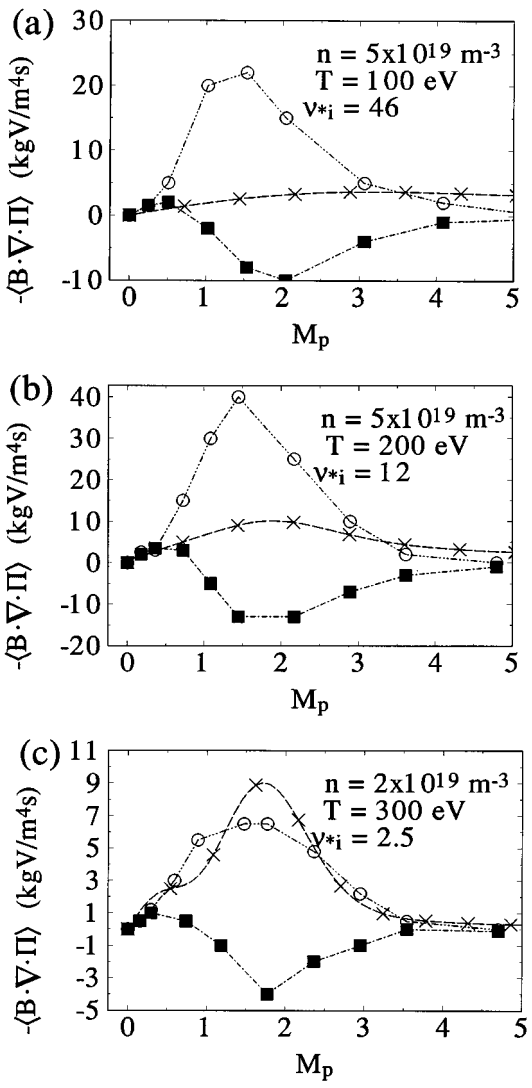

Figure 7. Parallel viscosity as a function of the radial electric field for temperatures (a) 100 eV and (b) 200 eV, with density $n = 5 \times 10^{19}$ m^{-3} and (c) for the low collisionality case with $T = 300$ eV and $n = 2 \times 10^{19}$ m^{-3} calculated with the ASCOT code (squares), from the expression of Shaing (crosses) and the sum of the RHS terms in Eq. (4) calculated with the ASCOT code (circles).

4. Conclusions and discussion

In this article, the neoclassical ion flux in the presence of a radial electric field (non-equilibrium poloidal rotation) is calculated using the Monte Carlo technique and is compared with analytic results. Qualitatively the results agree, and quantitatively the results are of the same order. Therefore, the analytic expressions should be valid for an order of magnitude estimate of the bifurcation condition near the $\nu_{\star i}$ region. It should also be noted that in experiments in TEXTOR [2] with an externally biased electric field, the return current was found to be between the expressions of Shaing and Stringer as found in the present work. To isolate the influence of the different approximations and assumptions made in deriving the analytic expressions, more work is needed. In addition, the standard neoclassical theory breaks down if the density scale length is short enough, which might be the case near the edge. In the numerical simulation of the parallel viscosity it was found that, for large poloidal Mach numbers, the parallel viscosity term has a different sign than the analytic expression, but with convection and compression terms the total effect is always to drive parallel rotation, which leads to the decay of poloidal rota-

tion. With small poloidal rotation, parallel viscosity also drives parallel rotation. As the primary goal here is the study of the ion orbit loss based bifurcation theory, instead of investigating the limits of the neoclassical theory, parallel work has concentrated on the development of the method of self-consistent calculation of the electric field profile at the edge. The aim was to iterate the electric field in the presence of a momentum and energy conserving collision operator, ion source for the return current, and orbit loss providing the force to sustain the rotation, meaning also that many of the heuristic assumptions in this work can be avoided. From this work [8, 9] one has found that the self-consistent radial electric field does not bifurcate at $\nu_{*i} = 1$, and that the shear in $\boldsymbol{E} \times \boldsymbol{B}$ rotation from the solution for the transition conditions of discharge 8044 at ASDEX Upgrade, i.e. at $\nu_{*i} = 3.8$, in fact is sufficient for turbulence stabilization according to the Biglari–Diamond–Terry criterion [22] for the observed L mode solution.

Acknowledgements

This work was supported by the National Technology Agency and the Academy of Finland, and was performed within the co-operation agreement between the TEKES–Euratom Association and IPP–Euratom Association. The authors are grateful to S. Sipilä at Helsinki University of Technology for the programming of the ASCOT code diagnostics of flux.

Appendix

Analytic expressions

The derivation of the neoclassical return current in Ref. [11] includes poloidal variation of the electrostatic field, density and temperature, and is based on full velocity integrals. Gradient and curvature drifts are included, but the finite orbit effects and the radial variation of the radial electric field along the particle orbits are neglected.

As the poloidal electric field is not taken into account in ASCOT, it is also neglected here, and the steady state neoclassical current in Ref. [12] can be written as

$$j_{NC,str} = -\frac{1}{2\pi B_0 R_0} \int_0^{2\pi} (p_\parallel + p_\perp) \sin\theta \, d\theta \qquad (7)$$

where R_0 is the major radius, B_0 the magnetic field at the axis, and $p_\parallel$ and $p_\perp$ are the parallel and perpendicular pressure, respectively. Using the expressions for $p_\parallel$ and $p_\perp$ given in Eqs (9) and (10) in Ref. [12], and assuming zero radial density gradients, we can write the sum of pressure components as

$$p_\parallel + p_\perp = \epsilon n T \left((1+2x^2)^2 \Lambda + 2x^2 - 1 + \frac{V_0(1-I)}{ir\nu - V_0} \right) \times \exp(i\theta) \qquad (8)$$

with $V_0 = -E_r/B$, $\epsilon = r/R$ and zeroth order (no poloidal variation) densities and temperatures n and T, respectively. The functions I and Λ are defined as

$$I(z) = \frac{1}{\sqrt{2\pi}} \int_{-\infty}^{\infty} \frac{w}{w - \sqrt{2}z} \exp\left(-\frac{w^2}{2}\right) dw$$

$$\Lambda = I[I + 2ixyI + (1-I)x/z]^{-1}$$

where $z = x + iy$, $x = E_r/v_{ti}B_\theta = M_p$ and $y = \nu_{*i}\epsilon^{3/2}$ with normalized collisionality $\nu_{*i} = \nu R q / v_{ti}\epsilon^{3/2}$ and ion–ion collision frequency ν. Under these approximations, θ integration in Eq. (7) is trivial, and by knowing that only the real part of the equation has physical significance, the radial current becomes simply

$$j_{NC,str} = -D \mathrm{Im}\left((1+2x^2)^2 \Lambda + \frac{1-I}{ir\nu - V_0} V_0 \right) \qquad (9)$$

where $D = nT\epsilon^2/2rB_0$ is related to the diffusion coefficient.

The expression for parallel viscosity by Shaing [13, 23] in the absence of temperature and density gradients can be written as

$$\langle \boldsymbol{B} \cdot \boldsymbol{\nabla} \cdot \boldsymbol{\Pi} \rangle = \frac{\sqrt{\pi}\epsilon^2}{4r} n m v_{ti} B I_p U_\theta \qquad (10)$$

where the poloidal flow velocity is $U_\theta = (U_\phi B_\theta - E_r)/B$. Neglecting the toroidal velocity U_ϕ the integral I_p is

$$I_p = \frac{1}{\pi} \int_0^\infty w^2 e^{-w} \int_{-1}^{1} (1 - 3\xi^2)^2 \times \frac{\chi}{(\xi - x/\sqrt{w})^2 + \chi^2} \, d\xi \, dw \qquad (11)$$

where $\xi = v_\parallel / v$ is the velocity pitch and $\chi = y\nu_T/\nu\sqrt{w}$. Here, ν_T is the collision frequency for anisotropy relaxation. Using the expression for ν_T given in Ref. [20], results in the Pfirsch–Schlüter regime obtained with a more complete collision operator have been reproduced within 20% [13]. The radial current to lowest order in ϵ, in the regime where Pfirsch–Schlüter effects are not significant, can be expressed in terms of the parallel viscosity as

$$j_{NC,sha} = -\frac{\langle \boldsymbol{B} \cdot \boldsymbol{\nabla} \cdot \boldsymbol{\Pi} \rangle}{B_\theta B} = -xD\sqrt{\pi} I_p. \qquad (12)$$

References

[1] Stringer, T.E., Nucl. Fusion **35** (1995) 1008.
[2] Cornelis, J., Sporken, R., Van Oost, G., Weynants, R.R., Nucl. Fusion **34** (1994) 171.
[3] Rozhanskii, V., et al., in Controlled Fusion and Plasma Physics (Proc. 18th Eur. Conf. Berlin, 1991), Vol. 15C, Part IV, European Physical Society, Geneva (1991) 287.
[4] Stix, T.H., Phys. Fluids **16** (1973) 1260.
[5] Hirshman, S.P., Nucl. Fusion **18** (1978) 917.
[6] Stringer, T.E., Phys. Fluids **13** (1970) 810.
[7] Shaing, K.C., Crume, E.C., Jr., Phys. Rev. Lett. **63** (1989) 2369.
[8] Heikkinen, J.A., Kiviniemi, T.P., Peeters, A.G., Phys. Rev. Lett. **84** (2000) 487.
[9] Heikkinen, J.A., Kiviniemi, T.P., Peeters, A.G., Plasma Phys. Control. Fusion **42** (2000) A185.
[10] Heikkinen, J.A., Sipilä, S.K., Phys. Plasmas **2** (1995) 3724.
[11] Stringer, T.E., Connor, J.W., Phys. Fluids **14** (1971) 2177.
[12] Connor, J.W., Stringer, T.E., Phys. Fluids **14** (1971) 2184.
[13] Shaing, K.C., Phys. Fluids B **2** (1990) 2847.
[14] Stringer, T.E., Nucl. Fusion **33** (1993) 1249.
[15] Itoh, S.-I., Nucl. Fusion **29** (1989) 1031.
[16] Shaing, K.C., Spong, D.A., Phys. Fluids B **2** (1990) 1190.
[17] Ma, S., Sydora, R.D., Dawson, J.M., Comput. Phys. Commun. **77** (1993) 190.
[18] White, R.B., Boozer, A.H., Phys. Plasmas **2** (1995) 2915.
[19] Hinton, F.L., Hazeltine, R.D., Rev. Mod. Phys. **48** (1976) 239.
[20] Hirshman, S.P., Sigmar, P.D., Nucl. Fusion **21** (1981) 1079.
[21] Shaing, K.C., Hazeltine, R.D., Sanuki, H., Phys. Fluids B **4** (1992) 404.
[22] Biglari, H., Diamond, P.H., Terry, P.W., Phys. Fluids B **2** (1990) 1.
[23] Shaing, K.C., Crume, E.C., Jr., Houlberg, W.A., Phys. Fluids B **2** (1990) 1492.

(Manuscript received 21 January 1999
Final manuscript accepted 18 May 2000)

E-mail address of T.P. Kiviniemi et al.:
Timo.Kiviniemi@hut.fi

Subject classification: F0, Ti